Available online at www.sciencedirect.com

ScienceDirect

Advances in Space Research 67 (2021) 87–101

ADVANCES IN SPACE RESEARCH
(a COSPAR publication)

www.elsevier.com/locate/asr

Radio and optical investigations of storm time evolution of post-midnight equatorial plasma bubbles (EPBs) and their drifts over Indian sector

O.B. Gurav [a,1], S. Sripathi [a,*], R.N. Ghodpage [b]

[a] Indian Institute of Geomagnetism, Navi Mumbai, 410218 Maharashtra, India
[b] Medium Frequency Radar, Indian Institute of Geomagnetism, Shivaji University Campus, Kolhapur 416004, Maharashtra, India

Received 9 June 2020; received in revised form 6 September 2020; accepted 9 September 2020
Available online 25 September 2020

Abstract

We investigated the spatio-temporal evolution of disturbed time post mid-night Equatorial Plasma Bubbles (EPBs) using Canadian Advanced Digital Ionosonde (CADI) located at dip equatorial station, Tirunelveli (8.73°N, 77.7°E, 0.23°N Dip. Lat.), an all-sky imager (ASI) observations at low latitude station Panhala (16.48°N, 74.6°E, 11.1°N Dip. Lat.) and Gadanki Ionospheric Radar Interferometer (GIRI) at Gadanki (13.5°N, 79.2°E; 6.5°N Dip. Lat.) which is situated at few degrees towards east and south of Panhala on 02–03 February 2017 night. During this night, IMF Bz showed its periodic variation starting from 16:00 UT to 23:00 UT accompanied by decrease in SYM-H to as low as −35 nT indicating the onset of weak magnetic storm. The analyzed results suggested that cause of post-midnight EPBs could be due to manifestation of fluctuating eastward/westward electric field due to combined under-shielding/over-shielding Electric Fields and disturbance dynamo electric fields that led to rise and fall of the F-layer over dip equator. Interestingly, the EPBs over Panhala showed eastward motion initially that quickly reversed to westward later. Along with westward motion they also started growing until 21:30 UT. However, most of these EPBs disappeared with time except the one that started descending/shrinking towards southern side (i.e. towards equator). The rising and shrinking of EPBs is found to be fairly correlated with the equatorial vertical drifts. The westward drift of EPBs at Panhala and its anti-correlation with vertical drifts has been confirmed from CADI zonal/vertical drifts. Accordingly, the study also investigated the role of storm induced vertical Hall electric field as a possible cause for westward drifts and its anti-correlation with vertical drifts. However, GIRI observations do not show any significant westward drift on this night at Gadanki suggesting that there is a longitudinal gradient in the zonal drift of these EPBs. In addition to longitudinal drift reversal, the latitudinal gradient in zonal drifts also has been noticed. The present work highlights the role of storm induced disturbances in the generation and evolution of post-midnight EPBs which is believed to be triggered by weak magnetic disturbances in the deep low solar minimum.

Keywords: Geomagnetic storm; Equatorial Plasma Bubbles (EPBs); Shrinking of EPBs

1. Introduction

Equatorial Plasma Bubbles (EPBs) are the optical signatures of post-sunset plasma density irregularities which are generated at the dip equator. Arise in the F-layer height around post-sunset sector due to pre-reversal enhancement (PRE) in zonal electric field provides the necessary condi-

* Corresponding author.
E-mail address: sripathi@iigs.iigm.res.in (S. Sripathi).
[1] Now at: Department of Physics, Bharati Vidyapeeth (Deemed to be University), Yashwantrao Mohite College of Arts, Science and Commerce, Pune, 411038 Maharashtra, India.

https://doi.org/10.1016/j.asr.2020.09.021
0273-1177/

tions to form the EPBs through the generalized Rayleigh-Taylor (RT) instability mechanism. The EPBs that are triggered in the evening sector over the dip equator evolve nonlinearly into higher altitudes and simultaneously maps to either sides of the dip equator along the magnetic field lines (e.g. Tsunoda, 1985). The EPBs can be seen as depleted density regions (dark bands) in the optical airglow emissions, evolving plasma plumes in VHF radars, depleted density bite outs in the in situ satellite measurement of ion density, depleted ionospheric total electron content (TEC) in the GPS TEC observations and range or frequency spread F traces in the ionograms in ionosondes (e.g. Ref. Woodman, 2009). These plasma density irregularities can pose severe threat to the satellite based communication and navigation systems by causing scintillations when radio signal passes through them. So, understanding the generation and evolution of EPBs is highly important and can be utilized in modeling its behavior for prediction/foresting purposes to improve the communication and navigation performances under the severe weather and space weather conditions. Investigators from several decades have reported numerous characteristics of EPBs such as its occurrence during quiet and disturbed conditions (e.g. Abdu et al., 2003; Makela, 2006; Sharma et al., 2017; Sripathi et al., 2018a), morphology and evolution (e.g. Rao et al., 1997; Makela and Miller, 2008; Tulasi Ram et al., 2017; Sun et al., 2017; Gurav et al., 2019), zonal drift patterns (e.g. Gurav et al., 2018; Immel et al., 2004; Taori and Sindhya, 2014; Wiens et al., 2006; Ghodpage et al., 2018) etc. using optical, radio and satellite measurements over different parts of the globe.

It is known that high latitude electric fields and winds under geomagnetic storms couple to the equatorial and low latitude ionosphere (e.g., Kelley et al., 1979; Kikuchi et al., 2000; Blanc and Richmond, 1980). While the convection electric field couples to the equator quickly through prompt penetration electric fields, disturbance dynamo electric fields and winds and waves affect the low latitudes rather slowly. These electric fields, winds and waves affect the equatorial and low latitude electrodynamics significantly under geomagnetic storms. The morphological studies on the EPBs suggest that occurrence of post-sunset EPBs can be suppressed during magnetic storms under westward electric field penetration (e.g. Abdu et al., 2009), but EPBs can be generated in the post-sunset and around mid-night hours during magnetic storms under eastward penetration (Ramsingh et al., 2015; Sripathi et al., 2018b). The generation or suppression of EPBs in the post-sunset or post-midnight also can be due to the orientation of disturbance dynamo electric fields (Blanc and Richmond, 1980). In addition, the occurrence of post-midnight EPBs could be also due to variable quiet-time electrodynamics. So, it is very important to understand the cause of these EPBs in the post-midnight as they can be observed either due to local phenomenon unique to that longitude under quiet times or due to storm-time electrodynamics. Hence, understanding the causes of these post-midnight EPBs are very much relevant. The EPBs that are observed in the post-midnight are also known as post-midnight irregularities (PMIs). These irregularities occur when the conditions are not favorable for the RT instability in the post-sunset hours. Further, it is known that PMIs occur most frequently during low solar activity periods (e.g. Candido et al., 2011; Otsuka, 2018). Various researchers have studied the post-midnight generation of EPBs using VHF radars (e.g. Patra et al., 2009; Otsuka et al., 2009), airglow imager (e.g. Sun et al., 2017; Sripathi et al., 2018b; Wu et al., 2019) and satellite observations (e.g. Yokoyama et al., 2011). Sastri (1999) observed F-layer height enhancement just before the occurrence of post-midnight EPBs during June solstice of low solar conditions, but he suggested that this height rise does not play any significant role in the post-midnight EPBs occurrence. Patra et al. (2009) also observed post-midnight Field Aligned Irregularities (FAIs) during July 2008, a low solar activity period over Indian sector using Gadanki Radar observations. Their analysis suggests that the observed post-midnight FAIs could be due to the manifestation of drift gradients and RT instabilities associated with Es layer formation at the bottom side. On the contrary, Sharma et al., (2017) found no significant variation in the EPB occurrences during equinox periods of low to high solar activity years of ascending phase of 24th solar cycle over Indian sector. Recently, Sripathi et al. (2018a) over the Indian longitude sector observed the suppression of EPBs during the recovery phase of the moderate geomagnetic storm while occurrence of EPBs before and after the day of storm. They suggest that the altitudinal/latitudinal variation of disturbance dynamo electric field might be responsible for such observed feature. Further, PMIs can be generated by under shielding electric field during dawn sector owing to an unusually delayed polarity reversal of the penetration electric field (Sripathi et al., 2018b). Wu et al. (2019) recently observed EPBs which are believed to be generated around sunrise in the recovery phase of the geomagnetic storm on the night of 06–08 November 2015 over Chinese longitude sector. Their airglow and GPS TEC observations show that the EPBs continued to develop even after sunrise and lasted for about 1 h after sunrise. They report that the observed EPBs move westward apart from usual eastward drift and concluded that the enhanced upward vertical plasma drift during this geomagnetic storm might have played major role in triggering the EPBs near sunrise. It may be mentioned that while the all sky imager at Kolhapur, a low latitude station measures the intensity of airglow emissions and their zonal movement in its field of view, Doppler ionosonde located at Tirunelveli, an equatorial station can provide Doppler drifts of the plasma irregularities in both vertical as well as zonal directions. HF coherent scatter radar located at Gadanki, an off equatorial region can provide information about altitude variation of plasma irregularities. It is believed that simultaneous observations of both optical and radio techniques can provide spatio-temporal evolution of EPBs and their associated dynamics in the pre and post-midnight sectors. Accordingly, in the present work, we use multi-instrument observations using both optical and radio techniques to investigate the generation of post-midnight EPBs and their spatio-temporal characteristics over Indian sector. It is believed that combined analysis of these radio and optical observations can provide better insights about the plasma dynamics.

2. Details of the instruments and data sets

We have utilized the data from three different instruments having both optical and radio techniques for the present study. The details about these instruments are described below.

2.1. All-sky imager at Panhala

An all-sky imager (ASI) has been installed at MF Radar Facility, Shivaji University, Kolhapur (SUK) by Indian Institute of Geomagnetism (IIG) under the scientific collaborative program between IIG and SUK to investigate the low latitude EPBs and its association to Mesosphere-Lower-Thermosphere (MLT) dynamics. The ASI data presented in this study were collected on campaign mode operation during the year 2017 at Panhala hill station (16.48°N, 74.6°E, 11.1°N Dip. Lat.) which is ~25 km west to Kolhapur and ~800 m above from sea level. ASI employs different filters such as OH band emission, OI 577.7 nm and OI 630.0 nm which usually come from different altitude range such as ~87 km, ~97 km and ~250 km respectively. A high resolution [1024 × 1024 pixels (i.e. 1 MP)], CCD based ASI has 140° operating field of view (FOV) over Panhala which covers horizontal distance of ~1200 km in diameter (Ref. Figs. 3a and 3b). A detailed information of ASI can be found elsewhere (e.g. Gurav et al., 2019). The all-sky raw images are processed using standard image processing method as described in past literatures (e.g. Garcia et al., 1997; Lakshmi Narayanan et al., 2009). The images are unwrapped and projected onto equidistant geographical grid at an altitude of ~250 km. The dark band seen in the images are the signatures of EPBs which drifts usually towards east. The zonal (east–west) drift of EPBs has been determined using scanning method proposed by Pimenta et al. (2001).

2.2. Canadian Advanced Digital ionosonde (CADI) at Tirunelveli

The CADI observations presented here were made at Tirunelveli (0.23°N dip. lat.) which is an equatorial station located at southern tip of India. It can be operated in both ionogram and drift modes (Ref. Sripathi et al., 2016). For the ionogram mode, the transmission of sounding frequencies is usually from 2 MHz to 16 MHz having resolution of few 100KHz which record the ionograms at every 10 min interval, while for the drift mode the system is operated at few fixed frequencies with high temporal resolution of ~1 min between two successive ionograms. The drift mode provides the 3D drift motion of the plasma irregularities. However, due to aspect sensitivity, we use only the vertical and zonal drifts to investigate the drift variability due to storm time electrodynamics. It may be noted that plasma density irregularities in the post-sunset and post-midnight produces refractive index gradients that can be detected using spaced receiver analysis in the advanced digital ionosondes. The CADI ionograms are also further analyzed in terms of isoheights/isofrequencies, foF2 (MHz)/h'F (km) and spread F to understand the F-layer height variations and the characteristics of ionospheric irregularities which are the manifestations of equatorial spread F as seen in the ionograms. Here, we use both drift observations as well as scaling of ionogram data during the 02–03 February 2017. We also scaled the equatorial spread F (ESF) information for the whole February month and these observations are used to interpret the observed features in optical data over Panhala.

2.3. Gadanki ionospheric radar Interferometer (GIRI) at Gadanki

GIRI stationed at Gadanki, an off equatorial site has ability to carry out the HF radar observations of small scale (~5m) plasma irregularities to study the plasma instability processes as well as impact of forcing from below the atmosphere/ionosphere and forcing from above by the Sun on these plasma irregularities. It operates at operating frequency of 30 MHz which is important to investigate the bottom side irregularities as well as spatio-temporal evolution of such irregularities to the top side of the ionosphere. Further, GIRI has provision to steer the RADAR beam in ±50° east–west direction perpendicular to magnetic field lines to study the evolution and spatial distribution of these small-scale plasma irregularities. But, unfortunately, this radar was not operated as steerable radar on 02–03 February 2017. It was operated under single beam mode. This system can also provide the Doppler velocity, spectral width and the drift pattern of the small scale irregularities. Unlike VHF radar/MST radar that operates at 53 MHz which is also located at Gadanki, this radar is completely dedicated to study the plasma irregularities in the E and F regions of the ionosphere. The complete system description and other details of the GIRI system are exclusively given by Patra et al. (2014).

3. Results and discussion

Here, we present multi-instrument observations using the radio and optical techniques to investigate the EPBs in the post-midnight sector and the role of geomagnetic activity in the generation and evolution of these EPBs concurrently at the dip equator and low latitude Indian regions on the night of 02–03 February 2017. On this night, the solar and magnetic activity levels as represented by

F10.7 cm solar flux and Ap index are 75 s.f.u and 21 respectively. The solar flux is at its lower levels but there is a signature of magnetic activity on this day. Accordingly, we have investigated further the interplanetary and geomagnetic activity variations to examine the storm parameters during this night. Fig. 1 depicts the temporal variation in (a) interplanetary magnetic field Bz (nT), interplanetary Electric field Ey (mV/m), (b) AE index and (c) Sym-H (nT) during 02–03 February 2017. At the bottom panel of Fig. 1(c), the red and blue horizontal bars denote the Spread F and EPB occurrences as revealed by ionosonde and ASI respectively. The local sunset time on this night was 13:00 UT (18:30 IST). During 14:30 UT to 16:30 UT, ionograms showed very weak Spread F echoes in the bottom side of the F layer but the spread in the echoes is started enhancing mainly after 18:00 UT and up to morning hours (red horizontal bar). Please note that the ESF irregularities at Tirunelveli as seen in the early night are very weak and the reflection height is well below the 300 km which mayn't be able to map to Panhala. Hence, the onset timing of the EPBs as seen at Panhala through ASI is different unlike equator. Another reason could be that the ASI is located at low latitude. Accordingly, we observed EPBs from 18:30 UT to 23:30 UT in ASI images over Panhala. However, please note that EPBs are very weak from 18:30–19:30 and hence are not used for further

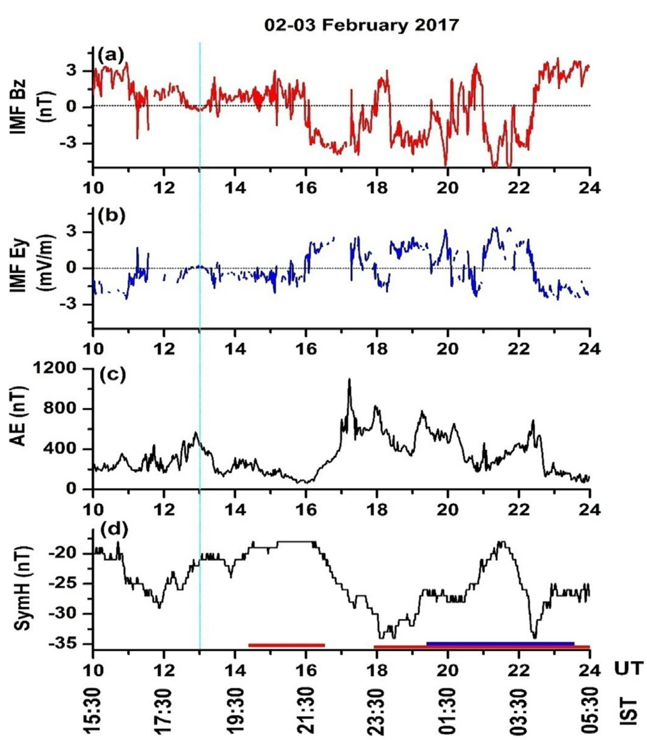

Fig. 1. Temporal variation of (a) Interplanetary magnetic field Bz (nT), (b) Interplanetary Electric field Ey (mV/m), (c) AE index and (d) Sym-H (nT) during 02–03 February 2017. The blue and red horizontal strips at the bottom indicate the duration of ESF and EPBs in CADI and ASI respectively. The vertical Cyan dotted line at 13:00 UT depicts the local sunset time. (For interpretation of the references to color in this figure legend, the reader is referred to the web version of this article.)

drift estimates. At a glance, from Fig. 1(a), it is seen that IMF Bz has three fairly periodic troughs between 16:00 UT to 24:00 UT. It is noted that, IMF Bz has sudden fluctuations in its second trough around ~20:00 UT which caused eastward penetration of electric field (see Fig. 1b) and at the same time EPBs were spotted at Panhala ASI. After 20:00 UT, EPBs started rising (developing) and drifted westward simultaneously and further one of the EPB shrinks around 21:30 UT. Detailed information regarding rising/shrinking shall be explained in the next section. In Fig. 1(c), AE shows maximum intensity fluctuations around 17:00 UT and approximately 3 h later we observed drift reversal of EPBs both at dip equator as well as at low latitude. This observed drift reversal could be the manifestation of storm time substorm disturbances that can move to the mid and low latitudes in terms of winds and electric fields due to auroral heating. Since auroral disturbances were present three hours prior to the local drift reversal, it is possible that disturbance dynamo winds and electric fields may also be playing roles on this night. Sripathi et al. (2018b) reported the EPB development arising from rapid increase in zonal electric field of eastward polarity due to under-shielding effect accompanied by southward IMF Bz turning around mid-night hours. This is unusual apart from results known so far. Also, they showed that this eastward polarity continued well towards sunrise apart from its usual westward polarity reported so far which is around 17:30 UT (23:00 LT). In present case IMF Bz changed its direction around 16:00 UT (21:30 IST) in first episode with eastward polarity. Again, in second episode around 18:00 UT (23:30 IST) southward turning occurred with eastward penetration apart from its usual westward polarity. The third episode around 21:00 UT (02:30 IST) also gave eastward penetration with little F layer height rise at the equator. Our present result showed the penetration electric field of eastward polarity accompanied by IMF Bz southward turning even well around midnight as well as towards pre-sunrise which caused the development of EPBs.

We also examined the percentage of occurrence of plasma irregularities for the whole month of February 2017 using Equatorial Spread F (ESF) irregularity patches in CADI ionosonde at Tirunelveli (top panel of Fig. 2) and EPBs observed in ASI over Panhala (middle panel of Fig. 2) to see whether occurrence of post-midnight EPBs on 02–03 February 2017 is a regular or rare phenomenon in this month. Similarly, the hourly occurrence of EPBs as observed in ASI is calculated by estimating the presence of EPBs at every one hour interval for the whole night observations. We have on an average 100 images recorded during observation. If out of 100 only 50 images show presence of EPBs, then the hourly percentage occurrence of EPBs on that night will be 50%. In case of ESF occurrence from ionosonde, a similar methodology is adopted. In the ionograms, the time interval is 10 min. For one hour data 06 ionograms are binned and the presence of ESF irregularity patches is noted. Accordingly, the hourly percentage

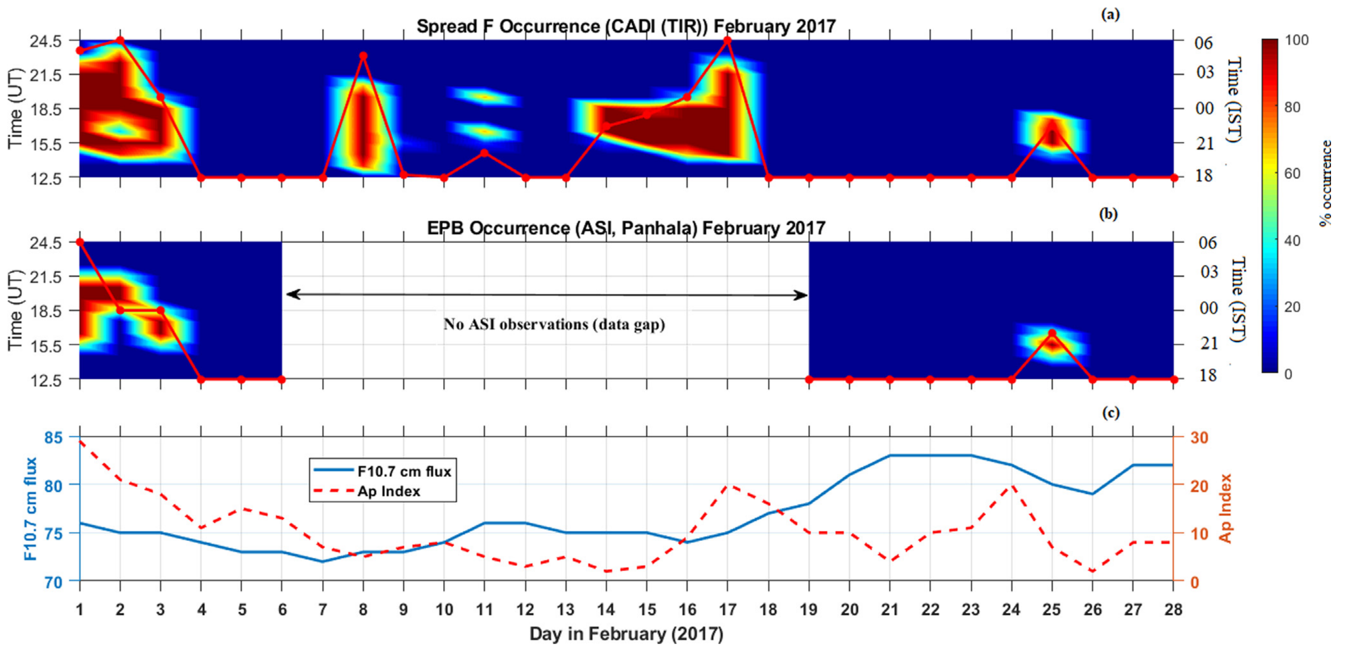

Fig. 2. Top panel shows the temporal variation of ESF occurrence calculated daily from ionosonde over Tirunevlveli, the middle panel shows the same, however, using ASI data and the bottom panel shows (a) Ap index and (b) solar flux at F10.7 cm respectively.

of ESF occurrence is calculated for the whole night. The mid-night timing is at 18:30 UT (00:00 IST) on the night of 02–03 February 2017. Please note that in addition to contour plots as mentioned above, we have also superposed the percentage of occurrence of ESF/EPBs shown in 'Red' color using CADI and ASI observations in respective plots to provide the day-to-day variability. The bottom panel in Fig. 2 indicates the daily solar (F10.7 cm flux) and magnetic activity (Ap index) variation during the entire month. It can be noticed from the solar and magnetic activity variations that while solar flux is steadily varied in the first 15 days having mean value of ~75 Solar Flux Units (sfu), however, it slowly increased little bit with mean value of ~82 sfu. In the same way, Ap index variation during this month suggest that it is below 20 throughout the month except during 1–2 February where it is ~30. Here it is seen that the ESF occurrence was seen in the early mid-night period on the night of 02–03 February 2017 which are only weak and intermittent while EPBs occurrence was spotted around mid-night when ESF is strong. But there is no onset of post-midnight EPBs on other days during the entire month. This suggests that post-midnight EPBs as seen on 02–03 February 2017 are unusual for this month. Fig. 3a provides the map of Indian region showing location of ionosonde at Tirunelveli, ASI at Panhala and GIRI at Gadanki. Fig. 3b depicts the sequence of ASI images over Panhala at ~06 min of time interval. In the image at 18:36 UT, we show vertical and horizontal strips of 20 pixels size which corresponds to north–south and east–west keograms. The top is north and left is west where distance (km) axis is also shown for reference. Around 19:34 UT, west tilted faint EPB structures are noted towards the southern part of FOV which are indicated by eastward yel-

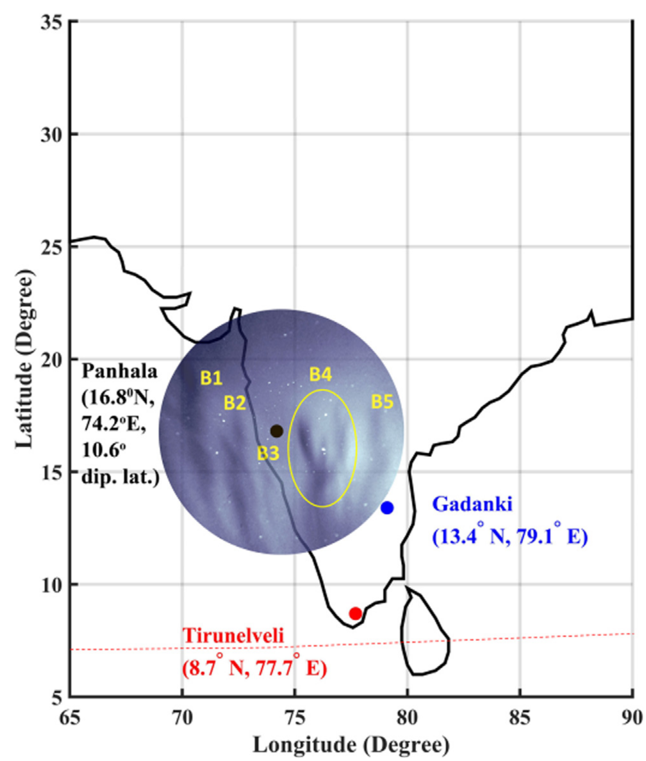

Fig. 3a. The all-sky imager and ionosonde are located at Panhala and Tirunelveli respectively. The Gadanki Ionospheric Radar Interferometer (GIRI) is located at Gadanaki. The circular image depicts the all-sky image with 140°field of view over Panhala covering area of about ~1200 km in diameter. The red dotted line indicates dip equator. (For interpretation of the references to color in this figure legend, the reader is referred to the web version of this article.)

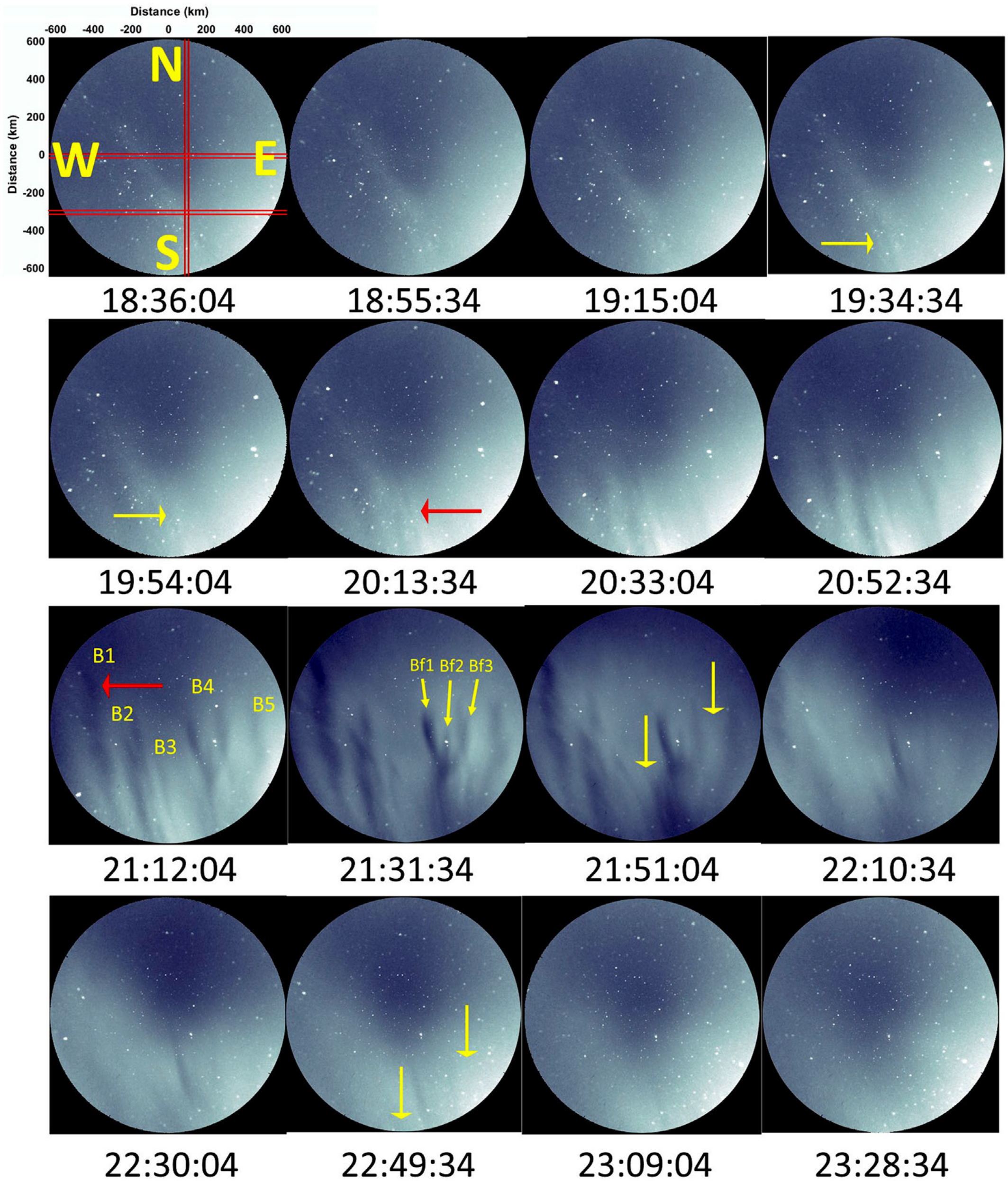

Fig. 3b. Sequences of OI 630.0 nm unwrapped images for the night of 02–03 February 2017 over Panhala. The equidistant projection and directions are depicted in first image at 18:36 UT (00:00 IST). The horizontal and vertical red lines depict the keogram cuts taken for EW and NS direction respectively. The yellow and red horizontal arrow depicts the direction of EPBs. (For interpretation of the references to color in this figure legend, the reader is referred to the web version of this article.)

low arrow. The EPBs show eastward drift momentarily during their onset. But, after ~20:00 UT they stopped their usual eastward drift and started moving westward as can be seen by red horizontal arrow. Interesting thing to note is that, with their westward drift they are simultaneously rising (poleward progression). The EPBs that were noted in the images have been classified as B1 to B5 from west to east. Out of these, B1 has attained maximum latitudinal extent. Further, B4 has come up with multiple branched structures around its top portion. We named them as Bf1, Bf2 and Bf3 from west to east. As time progresses we observe clear shrinking of whole B4 structure which is indicated by vertical downward arrow. All other westward moving EPBs vanish completely before the end of the observation period. The EPB B4 has reduced their westward drift while collapsing to south side. In a nutshell, the quick rising and shrinking of EPBs is observed for a very short duration from 20:00 to 23:00 UT. This can be more deeply understood by plotting the keograms and calculating the drift of EPBs from the sequential traces of EPBs in the scanning data. Figs. 4a, 4b and 4c shows the east–west keogram at 0 km (i.e. through zenith of the image), east–west keogram at −300 km (i.e. towards south) and north–south keogram at +100 km (i.e. towards east)

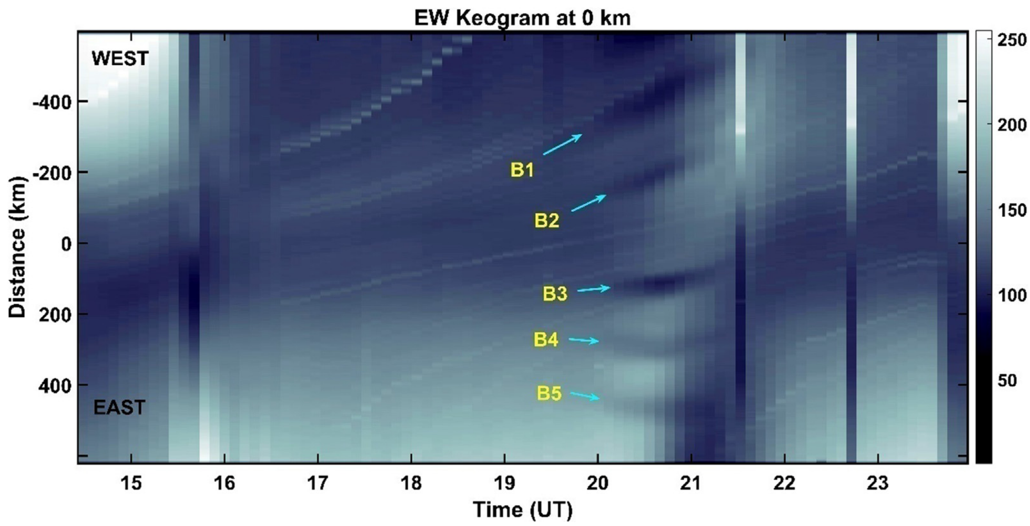

Fig. 4a. East-west keogram at 0 km (i.e. zenith) on 02–03 Feb 2017. The cyan marked arrows indicate EPBs. (For interpretation of the references to color in this figure legend, the reader is referred to the web version of this article.)

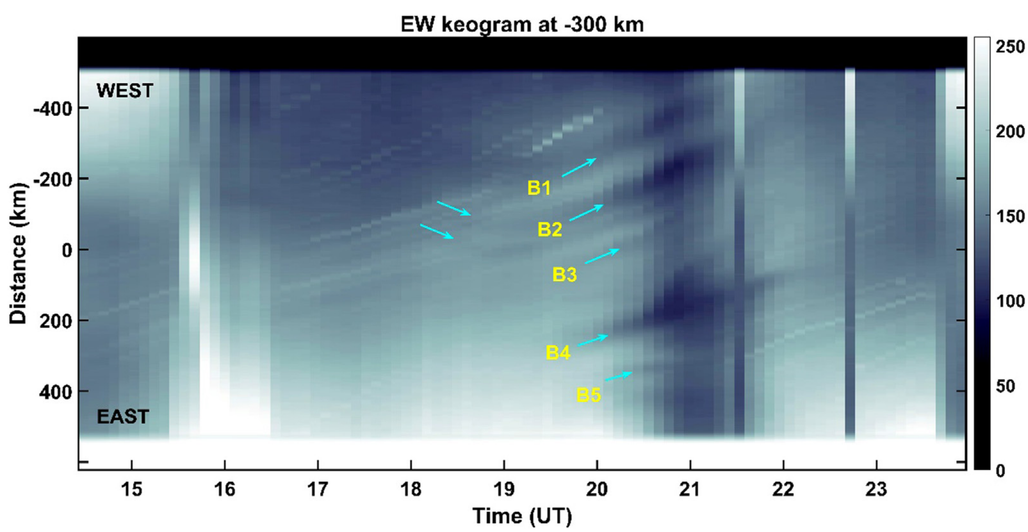

Fig. 4b. East-west keogram at −300 km (i.e. towards south) on 02–03 Feb 2017. The cyan marked arrows indicate EPBs. (For interpretation of the references to color in this figure legend, the reader is referred to the web version of this article.)

respectively. In Fig. 4a, five EPBs were observed between 20:00 to 21:30 UT marked by cyan arrows. With the closer look at observations, it can be seen that B4 and B5 which persists toward the eastern side of FOV of the image exhibits eastward drift at their onset. Further they drifted towards westside after 20:30 UT. However, other EPBs such as B1 to B3 move westward as soon as their onset is observed in ASI images. Interesting thing to note here is that the slope of all these EPBs from B5 to B1 seems to be increasing which means that the westward drift is increasing from eastern longitude to western longitudes. This demonstrates that there is a gradual increase of the westward drift associated with EPBs from east to west longitude sector and it further enhances during this magnetic disturbance. This can be treated as longitudinal drift variability of EPBs. Fig. 4b shows the east–west keogram taken at −300 km towards south of the image where the scenario is bit unclear with respect to the drift pattern. Here, except B5, all other EPBs tend to move westward. This is in contrast with the drift of B4 and B5 seen at 0 km keogram (Fig. 4a). This gives the evidence that there also exist a latitudinal gradient in zonal drifts where southern part of EPBs are moving westward while the middle part of EPBs were moving eastward first and then suddenly turned westward. This indicates that the effect of magnetic disturbance is maximum at dip equator than at low latitudes. However, in Fig. 4b the tails of B2 between 18:30 to 19:30 UT seems to be slightly drifting from the west to east. That means EPBs first drifted eastward, then reduced their drift speed and started moving towards west. While initial onset of EPBs has eastward drift with lower apex altitude, the apex altitude of the EPBs that moved from east to west is higher

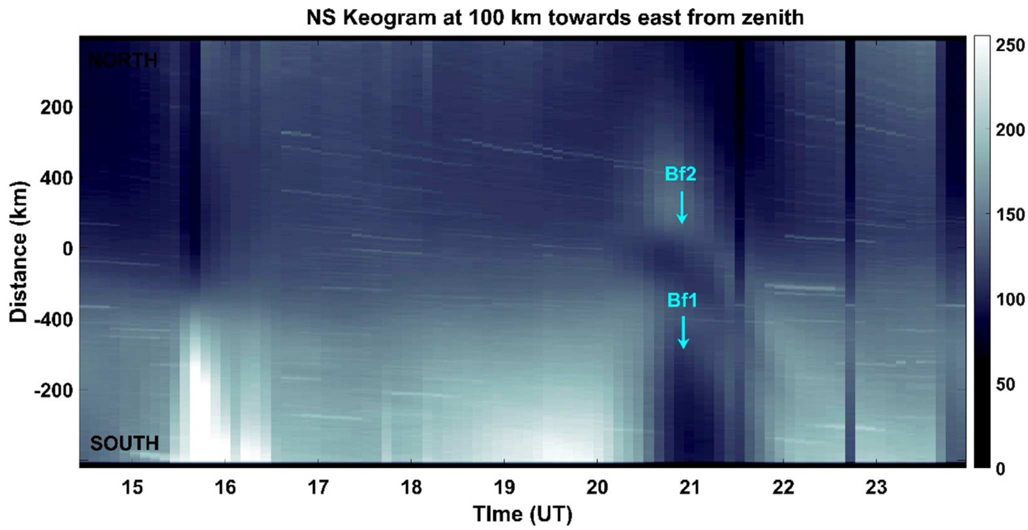

Fig. 4c. North-Southkeogram at +100 km (i.e. towards east) from zenith on 02–03 Feb 2017. The cyan marked arrow indicates EPB (Bf1 and Bf2) shrinking towards south. (For interpretation of the references to color in this figure legend, the reader is referred to the web version of this article.)

due to their altitudinal development. Fig. 4c shows the north–south keogram taken at 100 km towards east side from the center of the image. In this Figure, shrinking feature of B4 (i.e. Bf1 and Bf2) is noted as downward motion of depletions. From Fig. 3b we see that B4 has three branched structures namely Bf1, Bf2 and Bf3. Out of which Bf3 vanishes immediately as time progresses while Bf1 and Bf2 persists until 23:00 UT in the all-sky images. The Bf1 reduces its westward drift and starts shrinking to equator after ~21:00 UT as shown by downward cyan arrow in Fig. 4c. To further understand deeply we have calculated drift speed of EPBs by measuring the longitudinal offset with respect to time as shown in Fig. 5. Fig. 5 depicts a) zonal drift on typical quiet night on 14–15 December 2017 (Ap index = 05); b) zonal drift measured at 0 km (i.e. zenith); c) zonal drift measured at −300 km; and d) rise/shrink speed of B4 (more specifically Bf1). This rise/shrink speed of EPBs is calculated by manual measurement

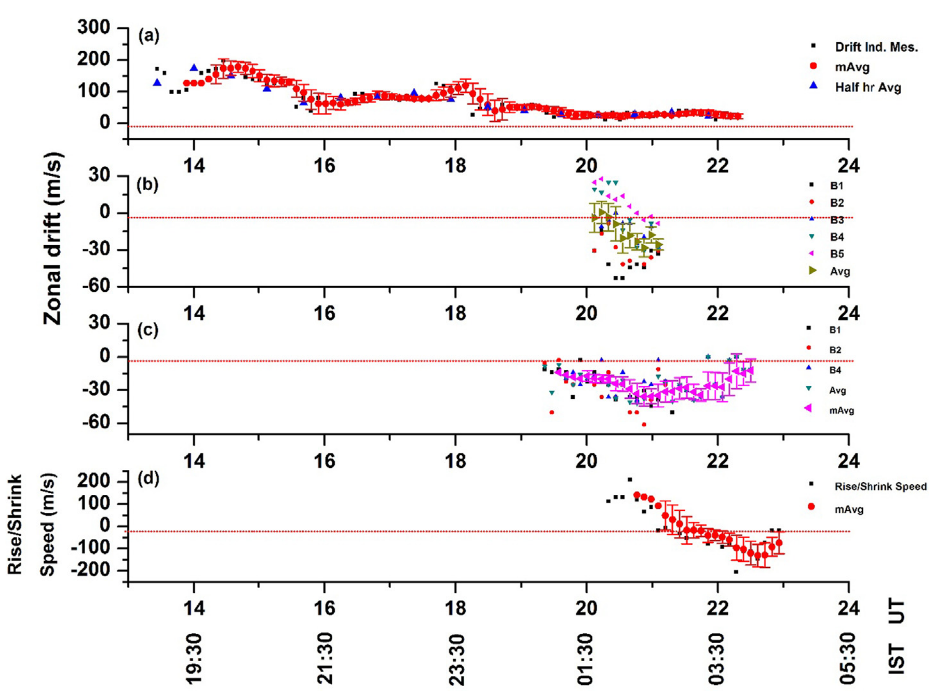

Fig. 5. a) The zonal drift velocity on typical quiet night of 14–15 December 2017 (Ap: 05), b) The zonal drift measured at 0 km (i.e. zenith) on disturbed night of 02–03 February 2017, c) The zonal drift measured at −300 km (i.e. towards south) on disturbed night of 02–03 February 2017 and d) The rise/shrink speed of B4 on 02–03 February 2017. The curves with error bars are the moving average of the data along with standard error. The other scatter data points are the individual measurements of the drift.

of poleward/equatorward movement of top portion of Bf1 from the sequential images of ASI. It is found that EPBs designated as B4 and B5 along zenith (0 km) shows eastward drift initially which then turned gradually westward (Ref. Fig. 5b). The average drift of all EPBs is westward after 20:00 UT and EPBs persisted up to 21:00 UT (over zenith line) which is why the drift is not available for further hours. But, drift speed of EPBs is available for about 19:30 UT to 22:30 UT at −300 km distance towards south from the zenith (See Fig. 5c). The EPBs observed at southern part of field of view (FOV) of the image move westward from 19:30 UT to as low as ~40 m/s and then slows down their westward drift after 21:00 UT towards morning hours. The top panel of Fig. 5 shows the drift variation calculated on a typical quiet night (14–15 December 2017) in the solar minimum year 2017. This night is specifically chosen because the EPBs occurrence in ASI images was more than 90% which is good to determine its nocturnal trend of zonal drift. From Fig. 5(a) it is seen that EPBs attain its maximum eastward drift just after sunset and gradually started decreasing towards early morning hours with no westward drift throughout the night. This is a typical quiet night zonal motion of EPBs over Panhala. However, the westward drift observed on the night of 02–03 February 2017 is indeed significantly different and could be due to influence of magnetic disturbance. Abdu et al. (2003)during the magnetospheric disturbance found that the irregularity drift initially towards east but slowly it reduced its eastward drift with time due to reduced vertical polarization electric field and suddenly it starts drifting westward which lasted up to pre-sunrise hours. Further, their results showed that both the topside and bottom side irregularities show westward drifts. In our case, we also observe the westward drift after 20:00 UT as can be noted in simultaneous records of CADI and ASI (CADI drifts will be discussed further). This implies that the large scale irregularities associated with EPB and smaller scale size structures embedded within the walls of EPBs and show similar trend in its zonal motion with different altitude domain. Fig. 5(d) indicates that the EPB (more specifically Bf1) starts rising after 20:00 UT and reaches maximum altitude at this time with rise speed of ~212 m/s but it started shrinking after 21:30 UT and reaches minimum shrinking speed of ~205 m/s. It can be suggested that the EPB (Bf1) rises and shrinks with almost same speed. Here, it is worthy to throw more light on quick rise and quick shrink feature which is observed on this night in Panhala ASI images. From the ASI image drift analysis (Fig. 5d), it is observed that EPBs started rising after 20:00 UT that continued to rise upto 21:30 UT and after that it started shrinking. Dao et al. (2016) suggested that most of the post-midnight FAIs do not reach an apex altitude of 450 km, but post-sunset FAIs grow faster to higher apex altitudes (above 500 km). But in our case the apex altitude of post-midnight EPBs is significantly maximum. We believe that, the rising/growing EPBs as seen in present study could be attributed to the bulk motion of plasma due to upward and downward motion of vertical drift as seen in the CADI drifts. Tulasi Ram et al. (2017) using Equatorial Atmosphere Radar (EAR), Kototabang reported that the vertical rise velocities of EPBs are considerably smaller (~26–128 m/s) around midnight period as compared to post-sunset period (~45–265 m/s). However, the rise speed of EPBs as calculated from ASI in present case has attained maximum speed of ~212 m/s during post-midnight itself is intriguing.

We have further analyzed zonal and vertical drifts as inferred from Doppler measurement of CADI ionosonde at Tirunelveli, a dip equatorial location. Fig. 6(a-d) shows temporal variation of (a) IMF Bz, (b) zonal drift, (c) vertical drift and (d) the no of scattering sources used to estimate the drift as obtained by CADI. In Fig. 6(a) the red and blue arrows indicate eastward and westward penetration of electric field. From Fig. 6(b), it is seen that the drift show fluctuating pattern up to 18:00 UT and after that it started displaying eastward drift up to 19:00 UT. Beyond that, eastward drift started reducing and becomes westward after 20:00 UT but this westward drift continued up to 22:00 UT. Moving onto Fig. 6(c), we see one prominent peak in vertical drift around 17:00 UT corresponding IMF Bz showed minimum value. This upward drift is associated with IMF Bz southward turning which is of eastward polarity (first red arrow around 16:30 UT). Around 20:00 UT the drift shows vertical progression (red upward arrow) where we observed the growth of EPBs over Panhala. Around 20:00 UT, IMF Bz has northward turning with fluctuating pattern which gave eastward penetration (Ref.

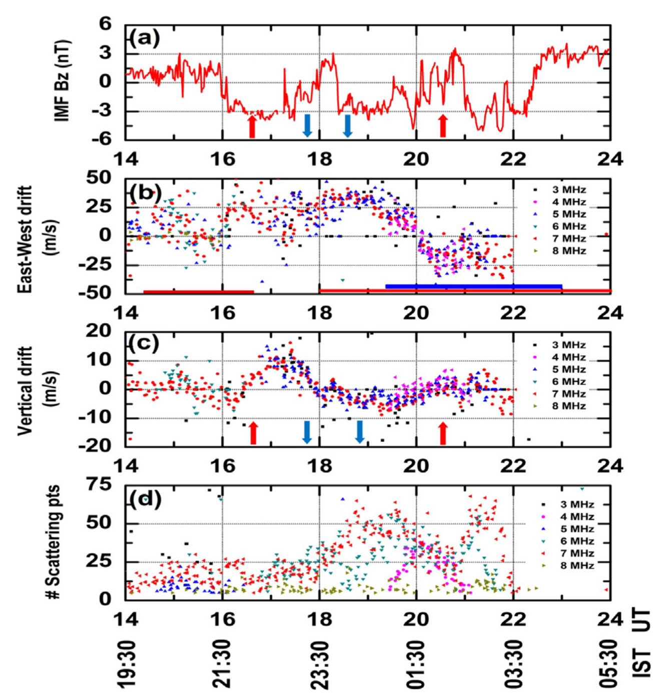

Fig. 6. The temporal variation of (a) IMF Bz, (b) east–west drifts, (c) vertical drifts and (d) number of scattering sources obtained from Canadian Advanced Digital Ionosonde (CADI) on 02–03 February 2017 over Tirunelveli. Indian Standard Time (IST) is shown in the bottom.

Fig. 6(a)) and consequently causes upward drift. Just prior to 21:00 UT, IMF Bz has sudden sharp southward turning which causes downward drift as noted by CADI (Ref. blue downward arrows around 21:00 UT). This may be due to the westward penetration of electric field. After 21:30 UT, the drift showed downward movement where we observed shrinking feature. In addition, disturbance dynamo electric fields and winds could also be playing on this night as westward drifts are noticed in the zonal drifts. The disturbance dynamo electric field may cause westward electric field in the evening to midnight hours. However, after post-midnight, it can turn into eastward electric field and can lead to upward drift. From present investigations, we suggest that the shrinking and rising motion in the EPBs could be caused due to downward/upward motion of ambient plasma due to both prompt penetration electric fields as well as disturbance dynamo electric fields. Further, it is seen that the rising and shrinking in EPBs as seen over Panhala matches fairly well with the Doppler drifts as obtained from CADI at Tirunelveli. Recently, Narayanan et al. (2016) reported an interesting observation of shrinking EPBs observed over same location Panhala using all-sky imager. The shrinking corresponds to reduction of EPB apex altitude over the dip equator. Their results showed that the speed of shrinking at the apex altitudes of EPBs is different than that of the bottom side vertical drifts unlike what we observed in our present investigation.

To understand the causes for this drift reversal, we have re-examined the F region dynamo mechanism. Usually, the eastward zonal winds in the post-sunset hours produce strong downward vertical electric field that in turn maps to low latitude. This electric field in the presence of strong E region conductivity gradient produces strong Hall polarization electric field which again maps back to equator as vertical electric field to cause strong PRE drifts. So, strong eastward drifts are often seen in the post-sunset to pre-midnight hours which slowly reduces as time progresses and becomes zero or weak westward in the dawn sector. However, these electric fields get disturbed due to strong auroral disturbances during geomagnetic storms. It is believed that causes for the low latitude drift reversal arises from three sources namely (a) zonal wind reversal due to Coriolis force that can cause westward drifts; (b) vertical Hall electric field arising from disturbances in zonal electric fields, E_{EW} and prompt penetration electric field depending upon its polarity; and (c) longitudinal conductivity gradient in the E region and or lower F region as suggested by Abdu et al. (2003). It may be noted that Abdu et al. (2003) investigated the disturbed time vertical and zonal drifts of irregularities using CADI and airglow imager over Brazilian sector and showed that the vertical rise velocity obtained from sequences of airglow depletion edges over Cachoeira Paulista (22.6°S) are in agreement with the drifts calculated from CADI over Fortaleza (3.9°S). In our case, From Fig. 5(d) and Fig. 6(b) it is seen that the rising and shrinking drifts as obtained from ASI and CADI respectively are fairly matching in time but the drift obtained from ASI show higher values (approx. ± 200 m/s). Because ASI measures the drifts of depleted density structures which can grow to higher altitudes but CADI measures the drift of ambient plasma at the bottomside of the ionosphere. Further, we observed negative correlation between the zonal and vertical drifts as obtained from CADI which means upward drifts are correlating with the westward drifts movement of the small scale irregularities (Please refer Fig. 6(b) and (c)). These results are in agreement with the previous studies such as Abdu et al. (2003) where they have mentioned that there could be a possible cause of Hall electric field behind the anti-correlated variations in zonal and vertical drifts of small scale irregularities. Abdu et al. (1998) also reported that there is anti-correlation between zonal velocity fluctuations and vertical velocity inferred from CADI under magnetospheric disturbances. The mechanism behind this involves production of Hall electric field (vertical) in E layer accompanied by enhancement in E region ionization. This electric field is mapped to F-layer and causes zonal velocity fluctuations. Further, Santos et al. (2016) observed drift reversal under significant magnetic disturbance due to prevailing AE activity which may have enhanced the particle precipitation in auroral zones. They found an excellent agreement in westward drifts inferred from ASI and CADI. They suggest that the zonal drift reversal was caused by an increase in the ratio $\Sigma H/\Sigma P$ accompanied by particle precipitation which is responsible for the development of vertical hall electric field. They also noted enhanced E region conductivity as indicated by sporadic E layer (i.e. increased ΣH) which produces vertical hall electric field. This has played dominant role in driving the westward reversal of EPBs drift. However, we don't have low latitude sporadic E layer observations to show that E layer conductivity is indeed modified on 02–03 February 2017 and EPBs were found to move westward due to this conductivity gradient in the narrow longitude. But we could see some density fluctuations in isoheight and isofrequency analysis on this night suggesting that F layer might have undergone density modulation. Also the anti-correlation between zonal and vertical drifts supports the view that there could be strong vertical Hall polarization electric field due to conductivity gradient along the Indian longitude. On the other hand, the westward zonal drifts could be driven mainly by disturbance dynamo winds as the time difference between AE peak i.e. 17:00 UT and time at which westward drift as seen at Kolhapur i.e. 20:00 is found to be nearly 3 h. The winds that are blown from the high latitudes as meridional winds towards equatorward can turn into westward due to Coriolis force and can cause westward drifts within time period of 3 h if these auroral disturbances are propagated at higher speeds than normal wind speeds recorded. Since this storm is noticed at low solar activity period where ionization density is very low and ion drag is reduced significantly, it is possible that even small disturbances in the auroral zones can travel at higher velocities and can affect the mid and low latitudes. Further, it is known that when

IMF Bz turns southward under geomagnetic storm, the region 1 (R1) field aligned currents (FAC) are often becomes more stronger than region 2 (R2) currents and the enhanced convection electric field under this condition enhances the eastward electric field at the equatorial and low latitude locations during day until post-sunset hours which is known as under-shielding condition due to penetration of additional eastward electric fields (Kikuchi et al., 2000). However, when the IMF Bz turns northward, the region 2 (R2) current becomes dominant than region 1 (R1) current which is known as over-shielding effect. Due to this over-shielding effect, westward (eastward) electric field penetrates during daytime (nighttime) to the low latitudes (Kelley et al., 1979). In addition, the disturbance dynamo electric fields which is driven by westward wind during magnetic disturbances, also affect the low latitude ionosphere (Blanc and Richmond, 1980). The electric fields as driven by disturbance dynamo oppose the regular Sq current such that it is westward during daytime and eastward during nighttime. Consequently, onset of the EPBs during nighttime could also be affected by the disturbance dynamo electric fields in addition to the over-shielding electric field. The response of the equatorial ionosphere to a severe geomagnetic storm on 15 July 2000 and suggested that abnormal descent of mid-night F layer height under westward prompt penetration electric fields under the background environment of eastward disturbance dynamo electric fields (Sastri et al., 2002). They have suggested that despite of eastward disturbance electric fields, strong prompt penetration of westward electric field produced downward drift and caused decent of F layer to 200 km per hour. If no eastward disturbance dynamo could have been present, it could have caused F layer height to descent to beyond 200 km per hour which is significant. In our observations, we do believe that there could be eastward disturbance dynamo electric field is well present. But addition of eastward/westward prompt penetration electric fields due to under-shielding and over-shielding effect caused significant modification in the equatorial electrodynamics. Accordingly, the occurrence of ESF/EPB in a given longitude becomes the balance between the eastward electric field due to disturbance dynamo effect and westward electric field due to over-shielding electric field. If westward electric field becomes stronger, one can notice suppression of plasma bubbles. However, if eastward electric field becomes more dominant, it is possible that F layer height to rise up to produce ESF/EPBs in the equatorial and low latitude ionosphere. To understand more about this storm and its impacts on the nightside of the equatorial ionosphere, we have investigated the response of the equatorial F region density over Tirunelveli to this weak magnetic disturbance using the temporal variations in (a) isoheights (fixed height variation), (b) isofrequencies (fixed frequency variation) along with (c) IMF Bz during 10:00 to 24:00 UT on the night of 02–03 February 2017 as shown in Fig. 7. As explained in Fig. 1, the IMF Bz shows three troughs that start at ~16:00 UT, ~18:00 UT and ~21:00

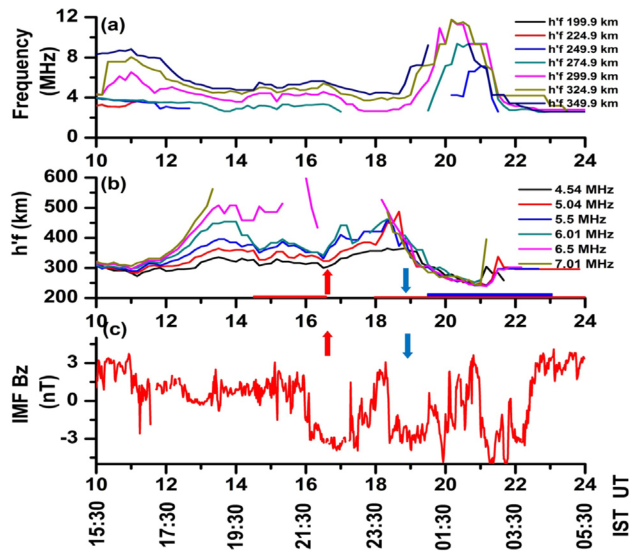

Fig. 7. The temporal variation of (a) frequency (density) undulations of ionosonde F region observations, which is at fixed (virtual heights) altitudes over Tirunelveli, (b) the temporal variation of heights (h’f) undulations of ionosonde F region observations which is at fixed (frequencies) over Tirunelveli, the blue and red horizontal strips at the bottom indicates the ESF/EPB occurrences inferred from CADI and ASI respectively and (c) IMF Bz variations during the night of 02–03 Feb 2017. Indian Standard Time (IST) is shown in the bottom.

UT respectively. Here, isoheights has its first peak around 13:30 UT which may be attributed to post-sunset pre-reversal enhancement. After an hour, ionograms show weak spread F irregularities. However, during the first IMF Bz southward progression, we noticed rise in height started at around 17:00 UT wherein no spread F is noted at Tirunelveli (Ref. red upward arrows). Just after 18:00 UT, second sudden sharp southward turning of IMF Bz is noted which is responsible for the corresponding decrement in *iso*-height that is accompanied by westward penetration electric field (Ref. blue downward arrows). On the other hand, we see some fluctuating pattern of IMF Bz while turning to north around 20:00 UT which have created strong eastward electric field. During this period, we observed growth of EPBs to greater apex altitudes which canbenoticed at lower latitude station, Panhala.Further, third sharp southward turning is seen in IMF Bz around 21:00 UT which again lifted the F-layer to slightly upward as can be seen in the Fig. 7(b). During the period of 19:00 to 22:00 UT, the F-layer was at almost around ~250 km which gave large number of scattering sources (Ref. Fig. 6(a) and (b)) for radio pulses of different frequencies sent by CADI from the dip equator. This ascertains that CADI drifts are reliable and can be used to compare with optical drifts. Also, during the same duration, airglow emission recorded at Panhala got intensified because the peak airglow emission height is assumed to be ~250 km (Ghodpage et al., 2014). So, whenever EPB aligns (maps) at this altitude (~250 ± 50 km), only then it can be captured in the all-sky imager as their footprints (i.e. dark depleted bands) in the increasing latitudes (Makela, 2006). It is true that assumption of steady ~250 km altitude for airglow emission may not be suitable for high solar activity periods where the layer height varies from 250 km to 450 km. As the present observations are under the low solar activity period, the h'F variation on this night is not significantly different as can be noticed in Fig. 8. Fig. 8 depicts (a) the individual h'f variation during international quiet days in February 2017 as well their averaged h'f on quiet days (b) the disturbed time h'f on the night of 02–03 Feb 2017, the blue and red horizontal strips at the bottom indicates the ESF/EPB occurrences inferred from CADI and ASI respectively and (c) the IMF Bz variations during the night of 02–03 Feb 2017. In Fig. 8(b), during initial time (i.e. around and prior to sunset terminator), the h'f show height fluctuations and height goes steadily down up to 16:30 UT. Further it starts increasing up to ~18:00 UT and just after 18:00 UT, height started decreasing up to 21:00 UT but in the form of steps. This is due to sharp southward turnings of IMF Bz around 20:00 UT. Further, around 21:00 UT again IMF Bz has sharp southward turning that causes slight increase in F-layer height. The post sunset rise (PSSR) of F layer (i.e. PRE) arises from different processes such as 1) AGWs propagating from bottom side up to thermospheric heights which can modulate the F layer. 2) Disturbed time PPEF and DDEF which modifies the low latitude ionosphere with their polarities similar or opposite with the existing night time electric field prior to PRE (before sunset) or in the mid-night period (Refer Abdu et al. (2018) and references therein). Here note that the 'red' and 'blue' arrows shown in the figure indicate the upward/downward drifts due to eastward/westward penetration electric fields. From investigations of ionospheric parameters in the present study, we suggest that the height rise prior to EPB onset was accompanied by southward turning of IMF Bz can cause eastward electric field penetration to equator and further we suggests that the rising of EPB structures as seen in ASI may be attributed to the storm-time eastward penetration electric field. As year 2017 falls under low solar activity year, it is possible that EPBs can be excited even at lower altitudes due to reduced density and collision frequency unlike high solar activity years where they are enhanced. Accordingly, though magnetic activity levels are weak, still it is possible to raise the h'f (km) to above certain threshold levels needed for low solar activity periods. This can initiate the EPBs even though F layer height on this night is below that of the high solar activity levels.

For the comparison purpose, we also utilized GIRI observations made from Gadanki which is also an off equatorial station. Fig. 9 shows the temporal variation of (a) Height-time variations in SNR (dB), (b) Doppler velocity (m/s) (line of sight) and (c) Spectral width (m/s) observations using GIRI over Gadanaki and (d) Zonal velocity (m/s) obtained from Digisonde observed on 02–03 February 2017. In Fig. 9(a) it is seen that the field aligned irregularities (FAIs) occurred around 02:00 LT (20:30 UT) however we observed EPBs onset around 19:30 UT (01:00 LT) in ASI over Panhala. This can be understood

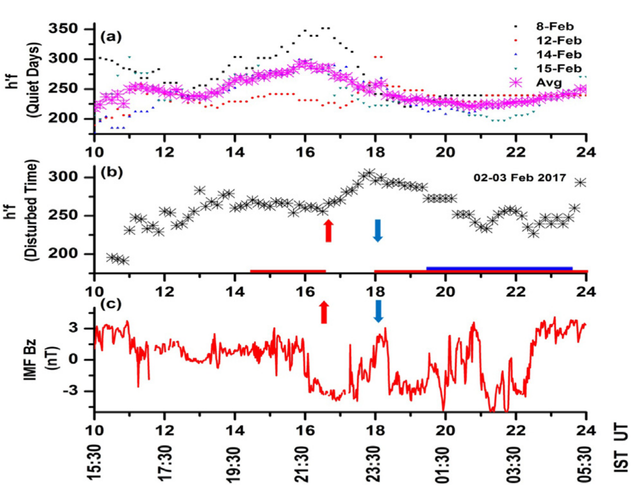

Fig. 8. The temporal variation of (a) h'f during international quiet days in February 2017 as well their averaged h'f on quiet days (b) The disturbed time h'f variations on the night of 02–03 Feb 2017. The blue and red horizontal strips at the bottom indicates the ESF/EPB occurrences inferred from CADI and ASI respectively, and (c) The IMF Bz variations during the night of 02–03 Feb 2017. Indian Standard Time (IST) is shown in the bottom.

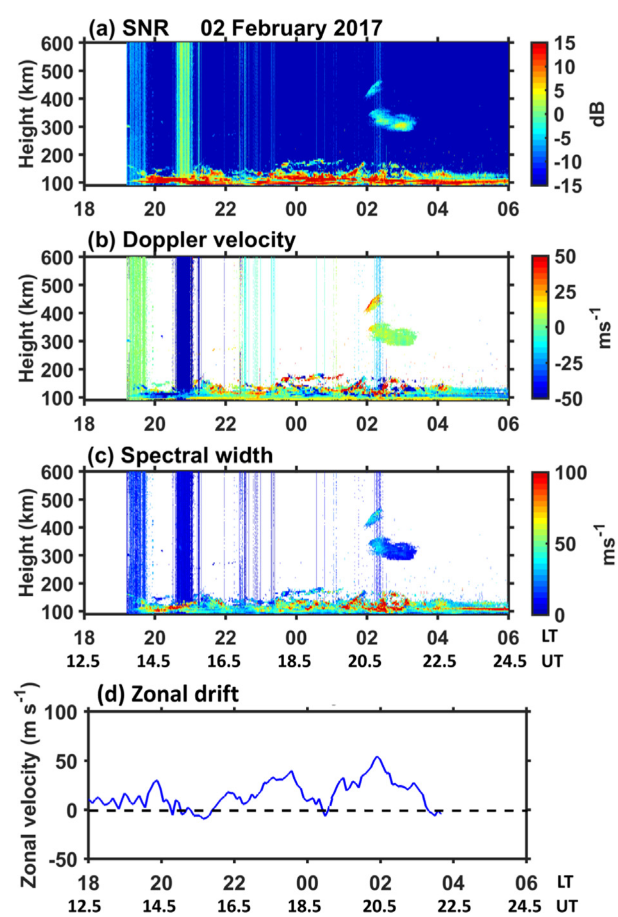

Fig. 9. The temporal variations of (a) Height-time variations of SNR (dB), (b) Doppler velocity (m/s), (c) Spectral width (m/s) as obtained using GIRI from Gadanaki and (d) Zonal drift velocity (m/s) as obtained from Digisonde from Gadanaki on 02–03 February 2017.

in a way that the EPBs initially found to drift eastward and their onset which was restricted towards the southern part of the FOV of ASI (Please see at 19:34 UT in Fig. 3b). Further, after 20:00 UT, EPBs started drifting westward as well as they were rising/growing. The EPBs which are confined to the western side of FOV (or western longitudes) have larger westward drifts than that of eastern side (or eastern longitudes). This can be confirmed from Fig. 4a. The growth of EPBs started at 20:00 UT and subsequently the FAIs are detected at Gadanki just after few minutes of its growth. Further, the EPBs confined to eastern side of FOV do not show large westward drifts. From the geometry (See Figs. 3a and 3b), it is understood that only B5 could be detected by GIRI over Gadanki. The characteristics of B5 is that it is unrecognizable in the southern part (-300 km) of ASI field of view and it is quite recognizable around zenith part (0 km) over Panhala. From Fig. 4a it is seen that, at zenith B5 show minimal eastward drift which further becomes almost stationary and it vanishes after 21:00 UT when shrinking behavior was in progress. Further signatures of B5 or surrounding irregularities can be seen in Fig. 9(a) which lasted towards dawn time (03:30 LT/22:00 UT). The Doppler velocities of FAIs show minimal or rather stationary drifts over Gadanki. The temporal variation of spectral width suggests that these FAIs were not fully developed and hence no strong turbulence is visible in the plasma structures. The zonal drift velocity (m/s) as obtained from Digisonde over Gadanki do not show any westward drift during the period of observation. From this analysis, we suggest that the drift reversal was influenced mainly over western longitude sector than that of eastern side. This indicates the presence of longitudinal gradient in the zonal plasma drifts during such weak magnetic disturbances when both prompt and disturbance dynamo are active. Further, it could be understood that the disturbance dynamo winds and electric fields could be dominant in the west but FAIs observed over Gadanki might not have been influenced significantly by the storm time disturbances leading to longitudinal drift reversals. In addition, it is believed that if substorm injection is prolonged for longer duration, the low latitude response due to prompt penetration will be masked by the disturbance dynamo electric fields (Abdu et al., 1997). They suggested that the longitudinal variability of the low latitude ionosphere in ionosondes and HF Doppler radars do exists under disturbance dynamo electric field (DDEF). They noticed strong westward electric fields in the post-sunset sector due to disturbance dynamo electric field that resulted in reduction of pre-reversal-enhancement (PRE) of the zonal electric field and also suppressed the plasma irregularities. However, they said due to eastward disturbance dynamo electric field in the post-midnight, it pushed the equatorial F layer to higher altitudes in the post-midnight sector. Despite eastward DD electric field in the post-midnight, ESF couldn't be noticed. This they have interpreted it as due to stabilization effect by the meridional winds.

To summarize, the analysis presented here brings out unique role of storm-time electrodynamics played around post-midnight that initiated EPBs and also simultaneously caused westward plasma drifts due the disturbance dynamo winds. However, upward and downward drifts could be associated with the combination of both disturbance dynamo electric fields of eastward and prompt penetration of eastward/westward electric fields as per the orientation of IMF Bz (IEFy). The results also confirm the presence of drift velocity reversals such as upward/-downward and eastward/westward drifts respectively. Such reports are available only over Brazilian sector. The rising and shrinking speeds of EPBs as noted in ASI over Panhala matches well with the vertical drifts inferred from CADI drifts which is not reported earlier. We have also noticed latitudinal/altitudinal drift shear and longitudinal variability of zonal plasma drift in a narrow longitudinal zone in our observations which are new. The role of under-shielding and over-shielding effects and disturbance dynamo electric fields are believed to be responsible for the longitudinal/latitudinal variation in the zonal drifts. We suggest that the contrasting zonal drifts such as eastward in the eastern longitudes and westward drifts at western longitude along with latitudes/altitudes could be associated with the conductivity gradients due to combined disturbance dynamo electric fields and prompt penetration electric fields.

4. Conclusions

We presented results of radio and optical investigations of storm time post-midnight EPBs that is observed on 02–03 February 2017 over Indian region during deep low solar minimum. The interesting aspect of this storm is that even though this storm is very weak, it could trigger the generation of equatorial plasma irregularities and EPBs at lower altitude (~300 km) which is well below the normal threshold value (around 375 km) for the h'f (km) under high solar activity years.

The main findings are summarized below:

a) The results suggest the occurrence of weak irregularities only in the ionosonde prior to post-midnight could be its occurrence at lower altitude that dissipated quickly due to strong collisions and hence couldn't be seen in other simultaneous observations of ASI and radar at low latitudes. However, post-midnight plasma irregularities are seen simultaneously when the h'F rose to above the threshold of ~300 km due to storm-time electric fields.
b) The results also suggest that the occurrence of post-midnight EPBs could be associated with the eastward and westward penetration of electric fields due to under-shielding and over-shielding effects of the magnetic storm around mid-night where the polarities usually gets changed for the shielding electric fields.

c) Though the storm event is very weak in terms of Dst and AE index, still the westward drift plasma drifts are noticed in our drift observations both in the ionosonde and airglow imager on the night of 02–03 February 2017. The westward drift as seen in this case could be associated with the storm-time disturbance dynamo winds and electric fields.
d) The growth of EPBs has continued and reached significant apex altitude around midnight hours (03:00 LT/21:30 UT) even though it is observed in the post-midnight period. Further, one of the EPBs started shrinking to bottom side (i.e. equatorward) when their upward growth has ceased. The EPBs rising/growing features as seen in the present analysis may be attributed to the storm-time eastward/westward penetration electric fields.
e) The rising and shrinking speeds of EPBs as noted in ASI over Panhala are matching very well with the vertical drifts inferred from Doppler measurement of CADI over equator (Tirunelveli) suggesting that vertical drift could be mainly responsible for this behavior.
f) The vertical and zonal drifts as obtained from CADI system shows anti-correlation i.e. upward drift corresponds to westward drift in our observations. Such observations are mainly reported from Brazil sector. So, our results confirm that eastward/westward drifts are anti-correlated with downward/upward vertical drifts respectively over Indian sector too.
g) The optical ASI observations show the presence of longitudinal gradient in the zonal plasma drifts due to weak magnetic storm which suggest that there could be longitudinal differences in the disturbance dynamo electric fields due to conductivity differences.
h) The observations by ASI also revealed the possibility of latitudinal/altitudinal shear in zonal plasma drifts in western longitude that could be due to spatial variability in the disturbance dynamo electric fields and may provide suitable conditions for the ESF/EPB onset.

Declaration of Competing Interest

The authors declare that they have no known competing financial interests or personal relationships that could have appeared to influence the work reported in this paper.

Acknowledgments

The lead author O.B. Gurav is highly grateful to the Director, Indian Institute of Geomagnetism (IIG), Navi Mumbai, India, for financial support through "Research Associateship". OBG also thanks V. L. Narayanan (The University of Arctic (UiT), Tromso, Norway) for providing necessary software programs for airglow image unwrapping. Thanks also go to S. Sau from IIG for the useful discussions. The interplanetary magnetic (IMF), Auroral Electrojet (AE) and SymH data are obtained from CDAWEB (https://cdaweb.gsfc.nasa.gov/cgi-bin/eval2.cgi). Geomagnetic data services from WDC, Kyoto Japan (http://wdc.kugi.kyoto-u.ac.jp/qddays/) are utilized. Authors are thankful to Dr P T Patil/Dr Vinit Erram, IIG for their help and support to operate the airglow experiments at Panhala, near Kolhapur, India on campaign modes. The funds for this research study are being provided by IIG, Department of Science and Technology (DST), Govt. of India, New Delhi. Authors are thankful to the technical staff of EGRL, Tirunelveli, for operating and maintaining the CADI. CADI ionosonde and ASI data used in this manuscript may be obtained by request to the Director, IIG. We would like to thank Dr. A. K. Patra, National Atmospheric Research Laboratory (NARL) for providing the GIRI radar maps and Digisonde plots at Gadanki that are utilized here. GIRI Radar and Ionosonde data at Gadanki may be obtained by writing to the Director, NARL, Gadanki.

References

Abdu, M.A., Batista, I.S., Takahashi, H., MacDougall, J., Sobral, J.H., Medeiros, A.F., Trivedi, N.B., 2003. Magnetospheric disturbance induced equatorial plasma bubble development and dynamics: A case study in Brazilian sector. J. Geophys. Res. Sp. Phys. 108, 1–13. https://doi.org/10.1029/2002JA009721.

Abdu, M.A., Kherani, E.A., Batista, I.S., Sobral, J.H.A., 2009. Equatorial evening prereversal vertical drift and spread F suppression by disturbance penetration electric fields. Geophys. Res. Lett. 36, L19103. https://doi.org/10.1029/2009GL039919.

Abdu, M.A., Nogueira, P.A.B., Santos, A.M., de Souza, J.R., Batista, I. S., Sobral, J.H.A., 2018. Impact of disturbance electric fields in the evening on prereversal vertical drift and spread F developments in the equatorial ionosphere. Ann. Geophys. 36, 609–620. https://doi.org/10.5194/angeo-36-609-2018.

Abdu, M.A., Jayachandran, P.T., MacDougall, J., Cecile, J.F., Sobral, J. H.A., 1998. Equatorial F region zonal plasma irregularity drifts under magnetospheric disturbances. Geophysical Research Letters 25 (22), 4137–4140. https://doi.org/10.1029/1998GL900117.

Abdu, M.A., Sastri, J.H., MacDougall, J., Batista, I.S., Sobral, J.H.A., 1997. Equatorial disturbance dynamo electric field longitudinal structure and spread F: A case study from GUAR/EITS Campaigns. Geophys. Res. Lett. 24 (13), 1707–1710.

Blanc, M., Richmond, A.D., 1980. The ionospheric disturbance dynamo. J. Geophys. Res. 85, 1669–1688.

Candido, C.M.N., Batista, I.S., Becker-Guedes, F., Abdu, M.A., Sobral, J.H.A., Takahashi, H., 2011. Spread F occurrence over a southern anomaly crest location in Brazil during June solstice of solar minimum activity. J. Geophys. Res. Sp. Phys. 116. https://doi.org/10.1029/2010JA016374.

Dao, T., Otsuka, Y., Shiokawa, K., Tulasi Ram, S., Yamamoto, M., 2016. Altitude development of postmidnight F region field-aligned irregularities observed using Equatorial Atmosphere Radar in Indonesia. Geophys. Res. Lett. 43, 1015–1022. https://doi.org/10.1002/2015GL067432.

Garcia, F.J., Taylor, M.J., Kelley, M.C., 1997. Two-dimensional spectral analysis of mesospheric airglow image data. Appl. Opt. 36, 7374–7385.

Ghodpage, R.N., Patil, P.T., Gurav, O.B., Gurubaran, S., Sharma, A.K., 2018. Ionospheric response to major storm of 17th March 2015 using multi-instrument data over low latitude station Kolhapur (16.8°N, 74.2°E, 10.6°dip. Lat.). Adv. Sp. Res. https://doi.org/10.1016/j.asr.2018.05.003.

Ghodpage, R.N., Taori, A., Patil, P.T., Gurubaran, S., Sripathi, S., Banola, S., Sharma, A.K., 2014. Simultaneous optical measurements of equatorial plasma bubble (EPB) from Kolhapur (16.8°N, 74.2°E) and Gadanki (13.5°N, 79.2°E). J. Atmos. Solar-Terrestrial Phys. 121, 196–205. https://doi.org/10.1016/j.jastp.2014.05.008.

Gurav, O.B., Narayanan, V.L., Sharma, A.K., Ghodpage, R.N., Gaikwad, H.P., Patil, P.T., 2019. Airglow imaging observations of some evolutionary aspects of equatorial plasma bubbles from Indian sector. Adv. Sp. Res. 64, 385–399. https://doi.org/10.1016/j.asr.2019.04.008.

Gurav, O.B., Sharma, A.K., Ghodpage, R.N., Nade, D.P., Chavan, G.A., Gaikwad, H.P., Patil, P.T., 2018. Zonal drift velocity of equatorial plasma bubbles during ascending phase of 24th solar cycle using all-sky imager over Kolhapur, India. J. Geophys. Res. Sp. Phys. https://doi.org/10.1029/2018JA025810.

Immel, T.J., Frey, H.U., Mende, S.B., Sagawa, E., 2004. Global observations of the zonal drift speed of equatorial ionospheric plasma bubbles. Ann. Geophys. 22, 3099–3107. https://doi.org/10.5194/angeo-22-3099-2004.

Kelley, M.C., Fejer, B.G., Gonzales, C.A., 1979. An explanation for anomalous equatorial ionospheric electric fields associated with a northward turning of the interplanetary magnetic field. Geophys. Res. Lett. 6, 301–304. https://doi.org/10.1029/GL006i004p00301.

Kikuchi, T., Luhr, H., Schlegel, K., Tachihara, H., Shinohara, M., Kitamura, T.L., 2000. Penetration of auroral electric fields to the equator during a substorm. J. Geophys. Res. 105, 23251–23252.

Lakshmi Narayanan, V., Gurubaran, S., Emperumal, K., 2009. Imaging observations of upper mesospheric nightglow emissions from Tirunelveli (8.7°N). Indian J. Radio Sp. Phys. 38, 150–158.

Makela, Jonathan J., 2006. A review of imaging low-latitude ionospheric irregularity processes. Journal of atmospheric and solar-terrestrial physics 68 (13), 1441–1458. https://doi.org/10.1016/j.jastp.2005.04.014.

Makela, J.J., Miller, E.S., 2008. Optical observations of the growth and day-to-day variability of equatorial plasma bubbles. J. Geophys. Res. Sp. Phys. 113, 1–7. https://doi.org/10.1029/2007JA012661.

Narayanan, V.L., Gurubaran, S., Shiokawa, K., 2016a. Direct observational evidence for the merging of equatorial plasma bubbles. J. Geophys. Res.: Space Phys. 121, 7923–7931. https://doi.org/10.1002/2014JA020025.

Narayanan, V.L., Gurubaran, S., Shiokawa, K., Emperumal, K., 2016b. Shrinking equatorial plasma bubbles. J. Geophys. Res. Space Phys. 121 (7), 6924–6935. https://doi.org/10.1002/2016JA022633.

Otsuka, Y., 2018. Review of the generation mechanisms of post-midnight irregularities in the equatorial and low-latitude ionosphere. Prog. Earth Planet. Sci. 5. https://doi.org/10.1186/s40645-018-0212-7.

Otsuka, Y., Ogawa, T., Effendy, 2009. VHF radar observations of nighttime F-region field-aligned irregularities over Kototabang, Indonesia. Earth, Planets Sp. 61, 431–437. https://doi.org/10.1186/BF03353159.

Patra, A.K., Srinivasulu, P., Chaitanya, P.P., Rao, M.D., Jayaraman, A., 2014. First results on low-latitude E and F region irregularities obtained using the Gadanki Ionospheric Radar Interferometer. J. Geophys. Res. Space Physics 119, 10276–10293. https://doi.org/10.1002/2014JA020604.

Patra, A.K., Phanikumar, D.V., Pant, T.K., 2009. Gadanki radar observations of F region field-aligned irregularities during June solstice of solar minimum: First results and preliminary analysis. J. Geophys. Res. Sp. Phys. 114, 1–10. https://doi.org/10.1029/2009JA014437.

Pimenta, A.A., Fagundes, P.R., Bittencourt, J.A., Sahai, Y., Gobbi, D., Medeiros, A.F., Taylor, M.J., Takahashi, H., 2001. Ionospheric plasma bubble zonal drift: A methodology using OI 630 nm all-sky imaging systems. Adv. Sp. Res. 27, 1219–1224. https://doi.org/10.1016/S0273-1177(01)00201-0.

Ramsingh, Sripathi, S., Sreekumar, S., Banola, S., Emperumal, K., Tiwari, P., & Kumar, B. S. (2015). Low-latitude ionosphere response to super geomagnetic storm of 17/18 March 2015: Results from a chain of ground-based observations over Indian sector. Journal of GeophysicalResearch: Space Physics, 120, 10,864–10,882. https://doi.org/10.1002/2015JA021509

Rao, P.B., Patra, A.K., Sarma, T.V.C., Murthy, B.V.K., Rao, K.S.V.S., Hari, S.S., 1997. Radar observations of updrafting and downdrafting plasma depletions associated with the equatorial spread F. Radio Sci. 32, 1215–1227.

Santos, A.M., Abdu, M.A., Souza, J.R., Sobral, J.H.A., Batista, I.S., 2016. Disturbance zonal and vertical plasma drifts in the Peruvian sector during solar minimum phases. J. Geophys. Res. Sp. Phys. n/a-n/a. https://doi.org/10.1002/2015JA022146.

Sastri, J.H., 1999. Post-midnight onset of spread-F at Kodaikanal during the June solstice of solar minimum. Ann. Geophysicae 17 (1111), 1115.

Sastri, J.H., Niranjan, K., Subbarao, K.S.V., 2002. Response of the equatorial ionosphere in the Indian (midnight) sector to the severe magnetic storm of July 15, 2000. Geophys. Res. Lett. 29 (13), 1651.

Sharma, A.K., Gurav, O.B., Chavan, G.A., Gaikwad, H.P., Ghodpage, R.N., Patil, P.T., 2017. Variation in occurrence of equatorial plasma bubbles (EPBs) using All Sky Imager from low latitude station Kolhapur (16.8°N, 74.2°E, 10.6° dip. Lat.). Adv. Sp. Res. https://doi.org/10.1016/j.asr.2017.09.014.

Sripathi, S., Abdu, M.A., Patra, A.K., Ghodpage, R.N., 2018. Unusual generation of localized EPB in the dawn sector triggered by a moderate geomagnetic storm. J. Geophys. Res. Sp. Phys. 123, 9697–9710. https://doi.org/10.1029/2018JA025642.

Sripathi, S., Banola, S., Emperumal, K., Suneel Kumar, B., Radicella, S. M., 2018. The role of storm time electrodynamics in suppressing the equatorial plasma bubble development in the recovery phase of a geomagnetic storm. J. Geophys. Res. Sp. Phys. 123, 2336–2350. https://doi.org/10.1002/2017JA024956.

Sripathi, S., Singh, R., Banola, S., Sreekumar, S., Emperumal, K., Selvaraj, C., 2016. Characteristics of the equatorial plasma drifts as obtained by using Canadian Doppler ionosonde over southern tip of India. J. Geophys. Res. Space Physics 121. https://doi.org/10.1002/2016JA023088.

Sun, L., Xu, J., Wang, W., Yuan, W., Zhu, Y., 2017. Evolution processes of a group of equatorial plasma bubble (EPBs) simultaneously observed by ground-based and satellite measurements in the equatorial region of China. J. Geophys. Res. Sp. Phys. 122, 4819–4836. https://doi.org/10.1002/2016JA023223.

Taori, A., Sindhya, A., 2014. Measurements of equatorial plasma depletion velocity using 630 nm airglowimaging over a low-latitude Indian station. J. Geophys. Res. Space Physics 119, 396–401. https://doi.org/10.1002/2013JA019465.

Tsunoda, R.T., 1985. Control of the seasonal and longitudinal occurrence of equatorial scintillations by the longitudinal gradient in integrated E region Pedersen conductivity. J. Geophys. Res. 90, 447–456. https://doi.org/10.1029/JA090iA01p00447.

Tulasi Ram, S., Ajith, K.K., Yokoyama, T., Yamamoto, M., Niranjan, K., 2017. Vertical rise velocity of equatorial plasma bubbles estimated from Equatorial Atmosphere Radar (EAR) observations and HIRB model simulations. J. Geophys. Res. Sp. Phys. 122, 6584–6594. https://doi.org/10.1002/2017JA024260.

Wiens, R.H., Ledvina, B.M., Kintner, P.M., Afewerki, M., Mulugheta, Z., 2006. Equatorial plasma bubbles in the ionosphere over Eritrea: occurrence and drift speed. Ann. Geophys. 24, 1443–1453. https://doi.org/10.5194/angeo-24-1443-2006.

Woodman, R.F., 2009. Spread F - An old equatorial aeronomy problem finally resolved? Ann. Geophys. 27, 1915–1934. https://doi.org/10.5194/angeo-27-1915-2009.

Wu, K., Xu, J., Yue, X., Xiong, C., Wang, W., Yuan, W., Wang, C., Zhu, Y., Luo, J., 2019. Equatorial plasma bubbles developing around sunrise observed by an all-sky imager and GNSS network during the storm time. Ann. Geophys. Discuss. 1–31. https://doi.org/10.5194/angeo-2019-122.

Yokoyama, T., Pfaff, R.F., Roddy, P., Yamamoto, M., Otsuka, Y., 2011. On post-midnight low-latitude ionospheric irregularities during solar minimum: 2. C/NOFS observations and comparisons with the equatorial atmosphere radar. J Geophys Res 116 (A11326). https://doi.org/10.1029/2011JA016798.